1-1-2015

Sonication-induced effects on carbon nanofibres in composite materials

Reece Gately
University of Wollongong, rdg604@uowmail.edu.au

Holly Warren
University of Wollongong, hwarren@uow.edu.au

Mattia Scardamaglia
University of Mons

Anthony C. Romeo
University of Wollongong, tromeo@uow.edu.au

Carla Bittencourt
University of Mons

See next page for additional authors

Sonication-induced effects on carbon nanofibres in composite materials

Abstract

The preparation and characterization of carbon nanofibre-gellan gum composite materials is presented. Electron microscopy analysis reveals that nanofibres are affected by sonolysis, i.e. fibre length reduces, while filling occurs. Spectroscopic analysis suggests that the nanofibres are modified during the preparation of the dispersions. It is shown that despite these effects, composite materials prepared using a short period of sonolysis (4 min) exhibit robust conductivity, strain at failure and Young's modulus values of 35 ± 2 S cm−1, 20 ± 1% and 1.3 ± 0.3 MPa, respectively.

Publication Details

Gately, R. D., Warren, H., Scardamaglia, M., Romeo, T., Bittencourt, C. & in het Panhuis, M. (2015). Sonication-induced effects on carbon nanofibres in composite materials. RSC Advances, 5 (25), 19587-19595.

Authors

Reece Gately, Holly Warren, Mattia Scardamaglia, Anthony C. Romeo, Carla Bittencourt, and Marc in het Panhuis

Sonication-induced effects on carbon nanofibres in composite materials

Reece D. Gately[1], Holly Warren[1], Mattia Scardamaglia[2], Tony Romeo[3], Carla Bittencourt[2], Marc in het Panhuis[1,4,*]

The preparation and characterization of carbon nanofibre-gellan gum composite materials is presented. Electron microscopy analysis reveals that nanofibres are affected by sonolysis, i.e. fibre length reduces, while filling occurs. Spectroscopic analysis suggests that the nanofibres are modified during the preparation of the dispersions. It is shown that despite these effects, composite materials prepared using a short period of sonolysis (4 min) exhibit robust conductivity, strain at failure and Young's modulus values of 35 ± 2 S/cm, 20 ± 1 % and 1.3 ± 0.3 MPa, respectively.

Introduction

The filling of carbon nanostructures such as carbon nanotubes (CNTs) has been investigated for applications including metal nanowires [1–3], hydrogen storage [4], energy storage [5], catalysts [6] and electrical insulation [7,8]. The methods used to fill CNTs can be broadly categorised as either chemical or physical. Chemical methods include functionalization [9] or electrochemical methods [5,10,11], whereas physical methods employ strong capillary suction within the CNTs [3,12–14]. CNTs are not readily filled as they are usually produced as closed structures resembling cylinders with hemi-spherical caps on either end. Opened CNT structures can be achieved through either direct growth [15] or by removing the caps [16–18]. Examples of the latter method include oxidative treatment [19] and boiling in acids [20].

The improvement of the mechanical [21,22] and electrical [23,24] characteristics of materials by incorporation of conducting carbon fillers is an active area of research. However, it is well-known that carbon fillers can be difficult to (homogeneously) disperse in aqueous solutions due their hydrophobicity and van der Waals interactions [25]. This disperse-ability issue has been successfully addressed by using dispersants (e.g. surfactants, polymers) in combination with sonolysis methods [26–28]. However, one of the drawbacks of sonolysis is that it can lead to damage to the carbon filler [29,30] and/or the dispersant [31]. In general, this results in a detrimental effect on the properties of the composite material [29,32–35]. For example, it has been shown that extensive sonolysis (21 hours) reduced the average CNT length from 3.5 μm to less than 0.5 μm [35]. This reduction in length was coupled with a significant decrease in the conductivity of the resulting CNT network. Furthermore, the detrimental effect of sonolysis on the molecular mass of polymers is well-known [36–41].

Here we investigate the effect of sonolysis on the properties of composite materials prepared by dispersing vapour grown carbon nanofibres (VGCNFs) with the biopolymer gellan gum. Gellan gum (GG, Scheme 1) is a linear, anionic, water soluble biopolymer which is derived from the bacteria *Sphingomonas elodea* (formerly *Pseudomonas elodea* or *Auromonas elodea* [42]). The repeating unit of the polymer is a tetrasaccharide, which consists of two residues of D-glucose and one of each residues of L-rhamnose and D-glucuronic acid. It is well-known for its applications in food technology ever since it was approved by the European Union and the United States Food and Drug Administration nearly two decades ago [43]. More recently, it has been demonstrated that gellan gum is an efficient dispersant for conducting carbon fillers such as carbon nanotubes, graphene and VGCNFs [44–47].

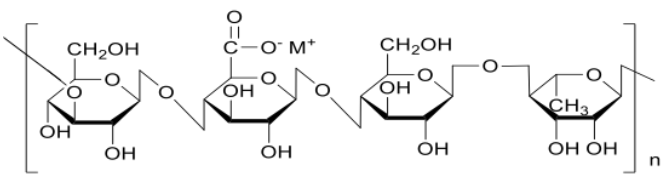

Scheme 1. Schematic representation of the molecular repeat structure of low-acyl gellan gum. M^+ indicated cationic counterions (e.g. Na^+).

VGCNFs are a conducting carbon filler material which were first manufactured in 1889 as a potential replacement for filaments in glow lamps [48]. Their structure was first elucidated in 1952 using electron microscopy, which showed stacks of highly graphitised carbon forming a tubular shape [49]. VGCNFs are produced by a catalytic thermal chemical vapour deposition technique with a floating catalyst [50]. This method produces two characteristic structures, (i) 'stacked cup' (or 'herringbone') structure, which looks similar to a series of graphite cups without bases stacked on top of each other, and (ii) a 'stacked deck' (or 'parallel' structure) which is a series of multiple concentric tubes of graphitised carbon (similar to those observed for multi-walled CNTs), but at a slight (approx. 4°) angle [51]. These structures are subsequently heat treated to remove (most of) the amorphous carbon outer layer and further

improve their physical, mechanical, and electrical properties [52]. It has been shown that conductivity and mechanical strength of the nanofibres is enhanced through heat treatment at 1500 °C [53]. VGCNF composite materials have been produced using poly(caprolactone), poly(urethane), poly(ethylene) and epoxy resins [54–61]. For example, recently it was demonstrated that shape memory properties of VGCNF-epoxy composite materials were enhanced by chemical functionalisation of VGCNFs [54]. Other potential applications include the use of VGCNFs as constituents in electromagnetic interference shielding materials as discussed in a recent review article [62].

In this paper, VGCNF-GG dispersions and composite (free-standing thin films) materials are prepared using sonolysis, vacuum filtration and evaporative casting. XPS/Raman spectroscopy, scanning electron microscopy, electrical and mechanical analysis was used to determine the effect of sonolysis on VGCNF graphitisation, average length, extent of opening, degree of filling, electrical conductivity, Young's modulus and ductility.

Experimental

Preparation of dispersions

Gellan gum was obtained from CP Kelco (low acyl form, Gelzan CM, Lot # 1I1443A). A GG solution (3 mg/mL) was prepared by adding 300 mg of GG to 100 mL of Milli-Q water (resistivity ≈ 18.2 MΩ cm) and heated to 80 °C on a hotplate (Stuart CB162 heat stirrer) while stirring with an overhead stirrer at ~800 rpm (IKA RW 20 digital) for at least 30 minutes.

Homogeneous dispersions were prepared by adding 100 mg of VGCNFs (Pyrograf Products, PR24-LHT, Batch info: PS1345 Box 8, HT 170, diameter up to 200 nm) to 10 mL GG solution (3 mg/mL) and applying horn sonolysis using a digital sonicator (Branson Digital Sonifier, power output 6 W, 0.5 s pulse, 0.5 s break between pulses). The microtip horn (Consonic, diameter 3.175 mm) was held 1 cm off the base of a 20 mL glass sample vial (diameter 25 mm).

Preparation of free-standing films

Buckypaper (BP) free-standing films were prepared by a vacuum filtration process. Briefly, 3 mL of the VGCNF dispersion (10 mg/mL VGCNF in 3 mg/mL GG) was diluted to 90 mL with Milli-Q water, resulting in final concentrations of 0.33 mg/mL and 0.1 mg/mL for the VGCNF and GG respectively. This was then subjected to bath sonication (50 Hz, FXP4, Ultrasonics) for 5 minutes. The dispersion was filtered through a commercial membrane (5 µm pore size, polytetrafluorethylene, Millipore) using a vacuum pump (CVC2, Vacuubrand) operating between 30 – 50 mbar. Once filtration had completed, the membrane was allowed to dry under controlled conditions (21 °C, 50% relative humidity, RH) in a temperature humidity chamber (Thermoline Scientific, TRH-150-SD) for up to 24 hours. Once dry, the BP was carefully peeled off the membrane to produce a free-standing film (diameter 40 mm).

Additional free-standing films were prepared by evaporative casting. Briefly, as-prepared dispersions were poured into a plastic petri-dish (diameter 55 mm) and allowed to dry under controlled conditions (21 ^{o}C, 50% RH) in a temperature-humidity chamber for up to 24 hours. The resulting films were then carefully removed from the substrate to produce free-standing films.

Electron Microscopy

Transmission electron microscopy (TEM) analysis of dispersions was performed using a transmission electron microscope (JEOL 2011) operated at an acceleration voltage of 200 kV. All images were captured on a TEM digital imaging system (Gatan Orius). A VGCNF dispersion was prepared by manual shaking of 10 mg VGCNF into ~20 mL of isopropanol (Sigma Aldrich Australia) for 1 min, hereafter referred to as 'unsonicated'. Dispersions (unsonicated and sonicated) were then cast into a copper grid (pore size 5 µm) and left to dry under controlled ambient conditions before TEM imaging. Scanning electron microscopy (SEM) analysis of all free-standing films was carried out using a field emission scanning electron microscope (FESEM JEOL JSM 7500-FA) operated at 5 kV and a spot size setting of 8. Length analysis of VGCNFs was performed using an image analysis package (Leica Application Suite Version 4.3).

Electrical Characterisation

Samples for electrical characterisation were prepared by cutting the films into small strips (3 mm x 25 mm), and contacted with conducting copper tape (3M) and conducting silver paint (SPI). A uniform pressure (~ 10^5 Pa) was applied to the electrode-sample contact area using bull clips (Officeworks, Wollongong). Current – voltage (*I-V*) profiles were obtained by measuring the current using a digital multimeter (Agilent 34410A) coupled with a cycling potential applied by a waveform generator (Agilent 3320A) in controlled ambient conditions (21 °C, 50% RH). The sample thickness was measured using a digital screw micrometer (Mitutoyo IP 65).

Mechanical Analysis

Tensile stress-strain measurements of the free-standing films were conducted using a universal mechanical testing apparatus (Shimazdu EZ-S). Films were cut into strips (width 4 mm) and a length assuring a gauge length of 10 mm. The samples were then stretched at a rate of 1 mm/min until failure.

Spectroscopy

Raman analysis was conducted using a Raman spectrometer (JY HR800, Horiba Jobin Yvon). The laser used was a HeNe laser (632.8 nm wavelength) at a power of 20 mW. The detector was an optical microscope (Olympus Bx41) with a spatial resolution of 1 µm. The spectrometer was calibrated using SiO_2 at a wavenumber of 520.7 cm^{-1}. All scans were performed between 500 and 3000 cm^{-1} under controlled ambient conditions.

X-ray photoelectron spectroscopy (XPS) was carried out in UHV conditions (base pressure in the 10^{-9} mbar range) using a spectrometer (VERSAPROBE PHI 5000, Physical Electronics), equipped with a hemispherical electron analyzer and monochromatic Al Kα X-Ray excitation source. The energy resolution was 0.7 eV. All binding energies were calibrated to the C 1s peak at 284.6 eV. The XPS spectra were deconvoluted into different chemical surroundings using commercially available software (CASA-XPS).

Results and Discussion

Electron microscopy

Carbon nanofibres were stabilised in gellan gum using a sonolysis process for up to 30 mins. TEM analysis (Figure 1a) of the as-received VGCNFs (unsonicated sample) revealed that the sample contained the characteristic 'parallel' (indicated with 1) and 'herringbone' (indicated with 2) structures. All of the imaged VGCNFs appear to be closed structures (see the example in Figure 1b), while a number of other types of carbon structures (e.g. amorphous carbon) are apparent. Although these other structures either completely cover the VGCNFs (Figure 1b) or partially cover the surface (Figure 1c), they are easily removed after only a short period (2 min) of sonolysis (Figure 1d-f).

Apart from removing the other types of carbon, sonolysis also resulted in opening the VGCNFs. For example, four VGCNFs can be identified in Figure 1d, of which the 'herringbone' structure is not damaged, but at least one of the three 'parallel' structures is open ended. Furthermore, we made the interesting observation that two of these VGCNFs appear to be filled. The enlarged view in Figure 1e clearly shows evidence of a filled VGCNF. Quantitative image analysis of TEM micrographs revealed that approximately 1/3 of the imaged VGCNFs appeared to be either completely or partially filled. However, analysis of dispersions prepared using longer sonication times (e.g. 30 mins) revealed that most of the imaged fibres were either filled and/or opened (sheared). For example, the VGCNFs in Figure 1g have been opened and are filled, whereas one of the fibres shown in Figure 1h has not been opened (and is therefore not filled). In addition, other fibres (such as the one shown in Figure 1i) revealed a fibre with the 'parallel' section filled and an undamaged (non-filled) 'herringbone' section. Examination of the TEM images shows that fibre damage and degree of filling increased with increasing sonication time.

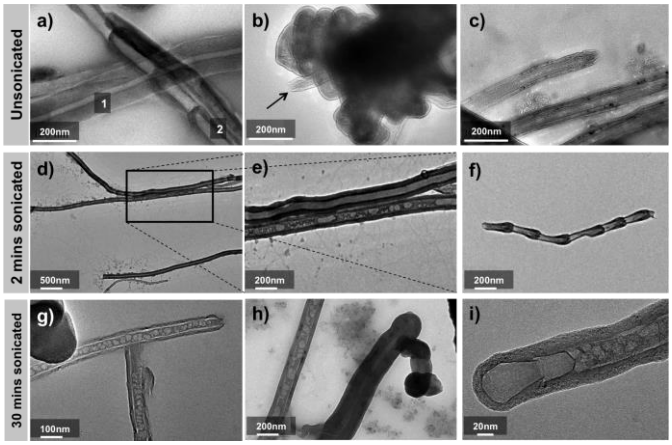

Figure 1. Typical high-resolution transmission electron microscopy images of VGCNFs unsonicated (a-c), sonicated for 2 min (d-f) and 30 min (g-i). a) VGCNF displaying the characteristic 'parallel' (1) and 'herringbone' (2) structures. b) VGCNF (indicated by arrow) completely covered with other types of carbon structures. c) VGCNFs partially covered with other types of carbon structures. d) Filled and un-filled VGCNFs. Rectangle indicates area of enlargement. e) Enlarged view of the filled and un-filled 'parallel' VGCNFs shown in image d). f) 'Herringbone' VGCNF with one open end. g) Filled 'parallel' VGCNFs. h) Filled and closed 'parallel' VGCNFs. i) A VGCNF with a filled 'parallel' section filled and an undamaged 'herringbone' end section.

Quantitative TEM analysis showed that the fraction of filled VGCNFs increased from 33% (after 2 min of sonolysis) to 85% after 30 min of sonolysis. This is further evidence that the filling effect is most likely due to the opening of the VGCNFs, i.e. whenever a fibre is damaged as a result of sonolysis, it is filled with the surrounding dispersant (gellan gum). We suggest that this is a result of capillary forces, as has been previously observed for carbon nanotubes [3,63].

The effect of the wall thickness was also examined quantitatively. It was found that after 2 minutes of sonolysis the VGCNFs with thinner walls were more likely to be sheared and filled, whereas the VGCNFs with the thicker walls were less likely to have been sheared. Figure 1e shows two fibres with different wall thicknesses; the top one is thicker and undamaged, whereas the bottom one is thinner and has been sheared and filled. This effect was personified after 30 min sonication; as previously mentioned, all VGCNFs that had been sheared were completely filled. It was found that all fibres with thin walls had been sheared, whereas fibres with thinner walls were less likely to be damaged. Figure 1h shows a filled fibre next to an unfilled fibre, and it can be seen that the right hand fibre was unfilled and not sheared, but has a significantly thicker wall compared to the fibre on the left, which has been sheared and filled.

SEM analysis of free-standing films (Figure 2) was used to assess the effect of sonication on the average length of the VGCNFs. After 2 min of sonication, it was found that the ends of the VGCNFs were reasonably circular in shape (Figure 2c), whereas after 30 min sonication the ends appeared to be more deformed and more ellipsoidal in shape (Figure 2d). At present it is not clear if the deformation is a direct result of sonolysis or

an in-direct effect due to fracturing. Further research is necessary to confirm this.

The length of the fibres decreased with increasing sonication times. For example, for free-standing films prepared by evaporative casting, the average length decreased from 3.2 µm (2 min sonication) to 1.5 µm (30 min sonication), see Figure 2e. This data exhibited a power-law ($y = mx^{-b}$) dependence with $b = 0.22 \pm 0.01$. Similar results (were obtained for films prepared by the vacuum filtration process (data not shown, power law exponent $b = 0.22 \pm 0.01$). This shortening through sonolysis is attributed to acoustic shearing as a result of inertial cavitation. The effect of this length reduction on the electrical characteristics is discussed in the next section.

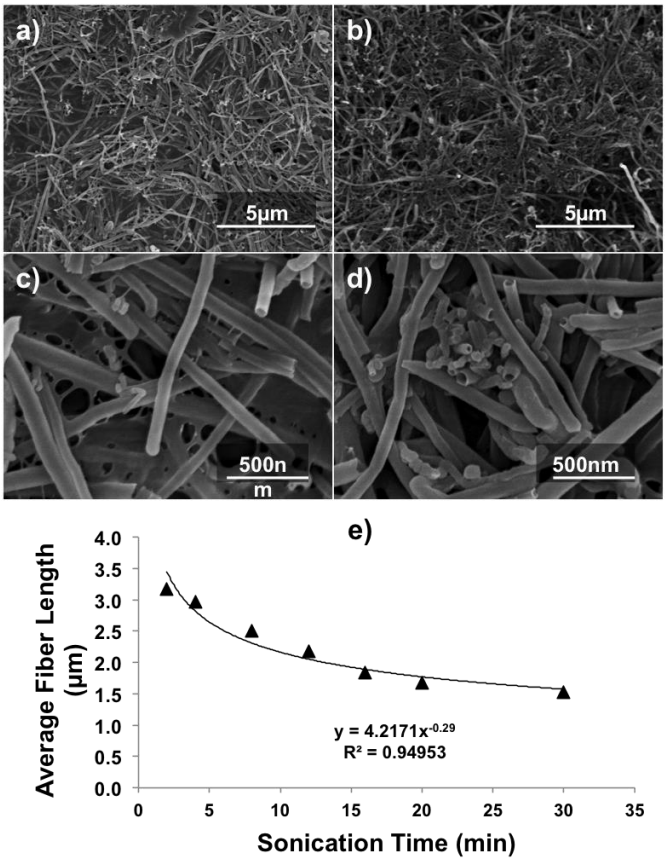

Figure 2. Typical scanning electron micrographs of free-standing films prepared by evaporative casting of dispersions prepared by sonicating for a) 2 min and b) 30 min. c) and d) are enlarged views of a and b), respectively. e) Average fibre length (assessed using image analysis on the micrographs) as a function of sonication time for films prepared by evaporative casting (triangles). The solid line is a power-law fit to the data.

Electrical and mechanical characterisation

The dispersions were used to prepare free-standing films by evaporative casting. The resulting free-standing films were used to assess the effect of sonolysis on the electrical and mechanical characteristics of these materials.

Films prepared by evaporative casting were used since they retain all of the VGCNF and the gellan gum materials present in the dispersion. In contrast, it is well-known that during the vacuum filtration process (to produce Buckypapers) some proportion of both the dispersant and carbon fillers are removed.

The current-voltage (*I-V*) characteristics of all free-standing films (tested under controlled ambient conditions) exhibited Ohmic behaviour, i.e. linear *I-V* characteristics. The total resistance (R_T) of the films was calculated from the *I-V* characteristics and plotted against film length (L) (Figure 3a). The conductivity was then evaluated by fitting the R_T versus L data to [41,45]:

$$R_T = L/(A_c\,\sigma) + R_C, \qquad (1)$$

where A_c, σ, and R_C indicate the cross-sectional area, conductivity and contact resistance (R_C), respectively. The slopes of the linear fits shown in Figure 3a for films prepared by 4 min and 30 min sonication correspond to conductivity values of 35 ± 2 S/cm and 25 ± 1 S/cm, respectively. Figure 3b shows that the conductivity decreased with increasing sonication time, exhibiting a plateau value for films prepared by dispersion that have been sonicated for at least 20 min. The decrease in conductivity could be fitted to a power-law ($y = mx^{-b}$), which yielded $b = 0.21 \pm 0.03$. Thus, there is good agreement with the power-law exponent as determined from the SEM analysis of length reduction (Figure 2e). This then could be seen as a validation of our SEM analysis.

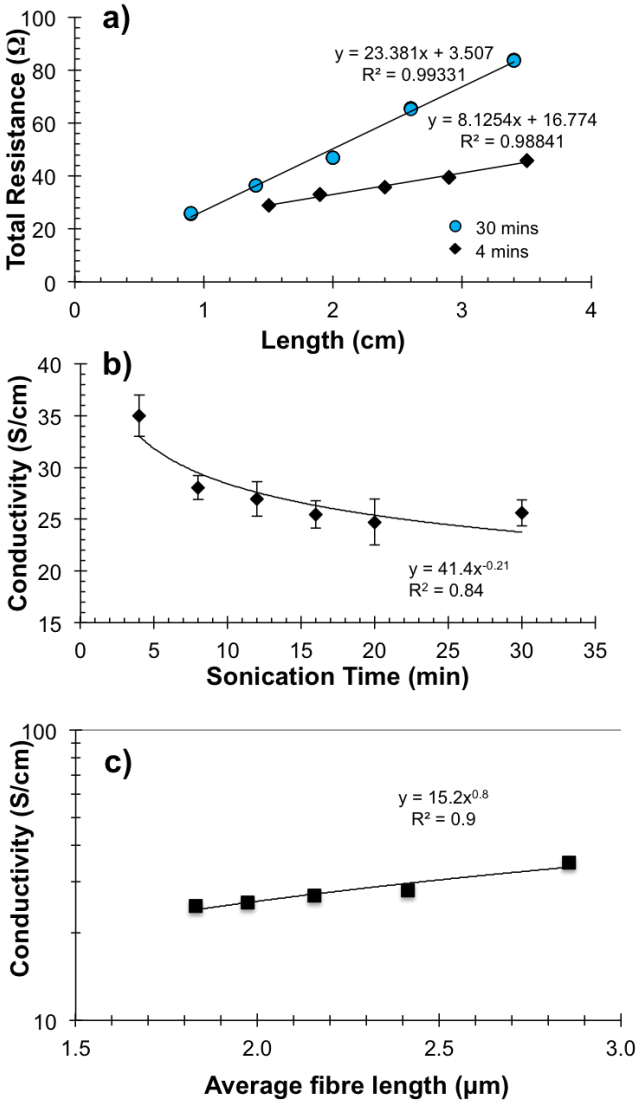

Figure 3. Electrical characterisation of free-standing composite films prepared by evaporative casting. a) Total resistance (21 °C, 50% RH) as a function of film length for films prepared by evaporative casting of dispersions sonicated for 4 (diamonds) and 30 (circles) minutes. b) Electrical conductivity as a function of sonication time. c) Conductivity as a function of average VGCNF length as determined by SEM analysis. Straight lines in a), b) and c) are linear fits to equation 1 and power law fit with exponent 0.8.

This behaviour is linked to the sonication-induced reduction in VGCNF length and can be explained as follows (similar to arguments used for carbon nanotubes as detailed in [35]); the VGCNFs form a percolative network in which the resistance is determined by a combination of the resistances along each of the VGCNFs and the junctions between the VGCNFs. It is relatively straightforward to determine which of these the dominant effect is. A reduction in the length of the VGCNFs is coupled with an increase in the number of junctions. Therefore, if the junction resistance is the determining factor in the conductivity of the film then it has been shown that the conductivity should follow a power law dependence on the length of the fibres [35]. In other words, conductivity decreases with increasing length of the fibres if junction resistance is dominant, while conductivity is independent of fibre length if junction resistance is neglible. Figure 3c shows that the conductivity as a function of fibre length follows a power law with exponent 0.8. Hence, the junctions between the VGCNFs dominate the electrical behaviour of the films.

Tensile testing was performed on free-standing films prepared by evaporative casting to assess the effect of sonication on the mechanical characteristics (Figure 4a). The Young's modulus decreased linearly with increasing sonication time from 1.3 ± 0.3 MPa (4 min sonication) to 0.21 ± 0.07 MPa (20 min sonication), see Figure 4b. This indicated that the films became more ductile with increasing sonication time, i.e. the films failed at a higher strain but lower stress. Previous research [32,41] has attributed this to a combined effect of damage to the polymer (shortening of the polymer chain length with increasing sonolysis) and the carbon filler (reduction in length as discussed above). The combined effect of this is a reduction in the Young's modulus and the tensile strength of the composite.

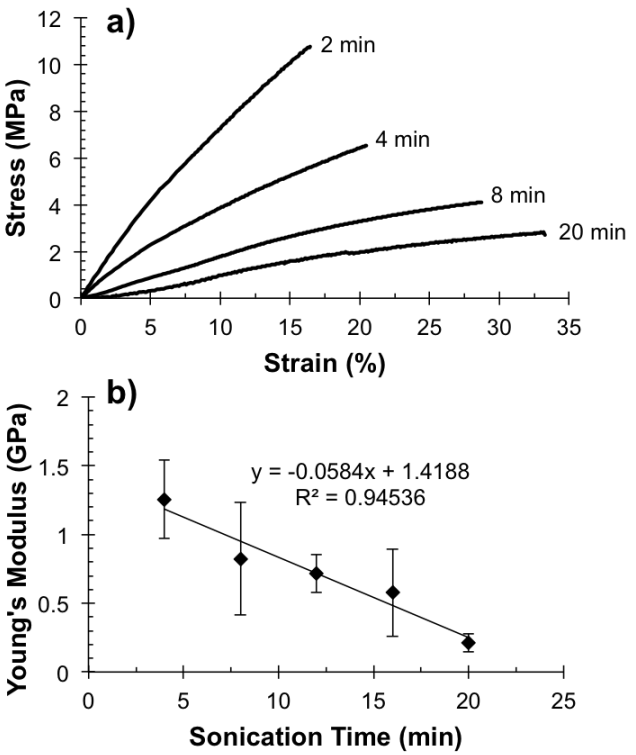

Figure 4. a) Typical tensile stress-strain plots of free-standing films prepared by evaporative casting of dispersions sonicated for 2, 4, 8 and 20 min. b) Young's modulus as a function of sonication time. The straight line in b) is a linear fit to the data.

It is clear that the reduction in the mechanical and electrical properties must be taken into account when using horn sonolysis. Our results indicate that 4 min of horn sonolysis results in composite materials which exhibit robust conductivity (35 ± 2 S/cm) and are mechanical sound. These values are comparable to conductivity values achieved for gellan gum composite materials with multi-walled carbon nanotubes (50 ± 5 S/cm), but (as expected) lower then with single-walled carbon nanotubes (110 ± 15 S/cm) [46]. Due to the smaller amount of

sonication time composite films with VGCNF have better mechanical properties compared to films prepared with carbon nanotubes.

Spectroscopy

Raman analysis was used to indicate the change in the level of graphitization of the VGCNFs due to sonolysis (Figure 5a). The spectra of the as-received VGCNFs (powder form), and free-standing films prepared by evaporative casting/vacuum filtration of dispersions exhibited two characteristic Raman bands at 1330 ± 2 cm^{-1} and 1579 ± 5 cm^{-1}, i.e. the D- and G-bands, respectively [63]. It is well-known that the ratio of the intensity of the D-band over intensity of the G-band, I(D)/I(G), is indicative of the level of graphitization. An increase in the I(D)/I(G) ratio corresponds to a decrease in the graphitization of the VGCNFs. The I(D)/I(G) data (Figure 5b) revealed that there is virtually no change and a small increase in the ratio with increasing sonication time for films prepared by evaporative casting and vacuum filtration, respectively. This appears to suggest that although sonication results in the opening of VGCNFs, it does not result in significant changes to the level of graphitisation. Inertial sonication brought about by sonication has been shown to perform similar effects with carbon nanotubes [64].

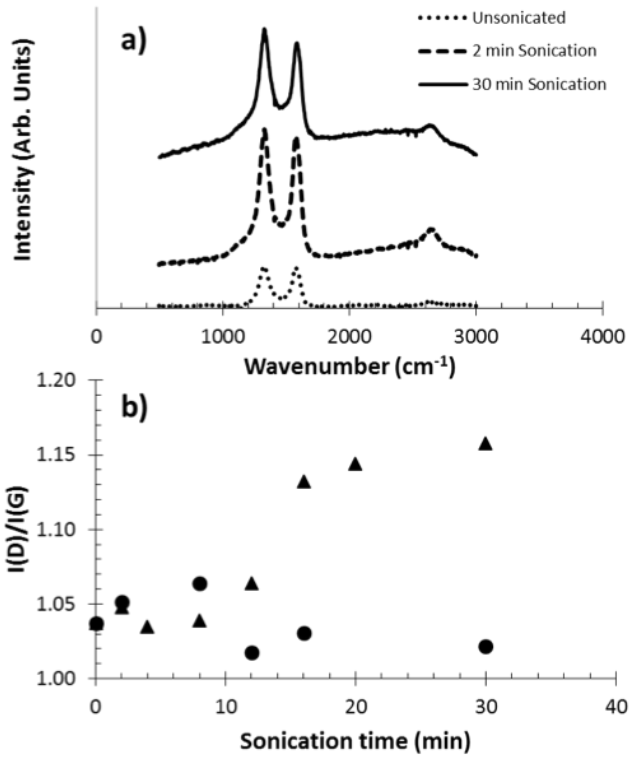

Figure 5. a) Raman spectra of VGCNF (unsonicated) and free-standing films prepared from dispersions sonicated for 2 min and 30 min. b) Ratio of the intensity of the D-band over the intensity of the G-band, I(D)/I(G) as a function of sonication time for free-standing films prepared by evaporative casting (triagles) and vacuum filtration (Buckypapers, circles).

As Raman has a depth of analysis large enough to probe the entire VGCNF and gellan gum does not exhibit suitable characteristic bands it is unlikely that this spectroscopic technique provides information about the effect of filling. To better understand the effects of sonication on the interactions between VGCNF and gellan gum in the dispersions, samples were characterised using XPS analysis. Figure 6 shows the typical XPS survey spectra recorded from unsonicated and sonication-treated VGCNFs (2 and 30 minutes, shown in figure). From the three spectra we can identify 2 main peaks which change their ratio: one at 284.4 eV, which is associated with photoelectrons emitted from carbon 1s core level and a second peak at about 533 eV generated by photoelectron emitted by O 1s core level.

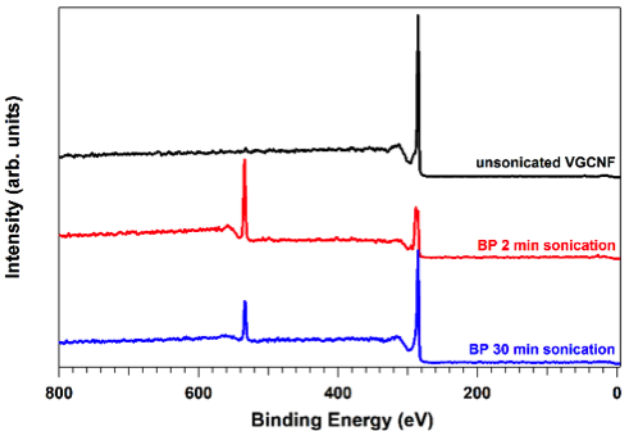

Figure 6. a) Typical C1s XPS survey spectra recorded on unsonicated VGCNFs (dotted line) and Buckypapers produced from dispersions prepared using 2-30 min of sonication (colored lines). The spectra are normalised and offset for clarity. b) Typical O1s XPS survey spectra recorded on unsonicated VGCNFs (dotted line, 10 times enhanced) and Buckypapers produced from dispersions prepared using 2-30 min of sonication (colored lines). c) Typical C1s XPS spectrum of Buckypaper prepared using a dispersion sonicated for 8 min. Numbers 1-6 indicate the deconvulotion of the signal using Gaussian components centered at 284.4 eV (sp2 bonded carbon), 285.0 eV (sp3 bonded carbon), 286.1 eV (hydroxilic oxygen) , 287.2 eV (carbonylic oxygen), 288.6 eV (carboxylic oxygen) and 290.6 eV (π-plasmon excitations), respectively. Black dots and red line indicate experimental data and the result of the fitting procedure, respectively. d) Oxygen content in the sample, obtained by the area under the O1s peak with respect to the C1s.

More information on the changes due to the sonication treatment can be understood from closer analysis of the C1s and O1s XPS spectra recorded on the different samples (Figure 7a-b). The pristine C1s spectrum (grey dotted line at the bottom of Figure 7a) centred at 284.4 eV has the typical asymmetric line shape of photoelectrons emitted from carbon atoms participating in sp^2 bonds. This asymmetry is associated with the many-electron response to the sudden creation of a photohole [65].

This spectrum also shows a second component at 290.6 eV associated with the electron energy loss due to π-plasmon excitations. The dispersion of the VGCNFs in gellan gum clearly results in a growing shoulder at the high binding energy side of the sp^2 peak. Figure 7c shows an example of the results of the curve fittings performed to explain the spectra of the sonicated samples. The modifications produced by the sonication treatment can be identified by a broad structure that peaks at 288 eV. This structure was previously attributed to photoelectrons emitted from carbon atoms belonging to carbon

functional groups singly and/or doubly bound to one or two oxygen atoms [66].

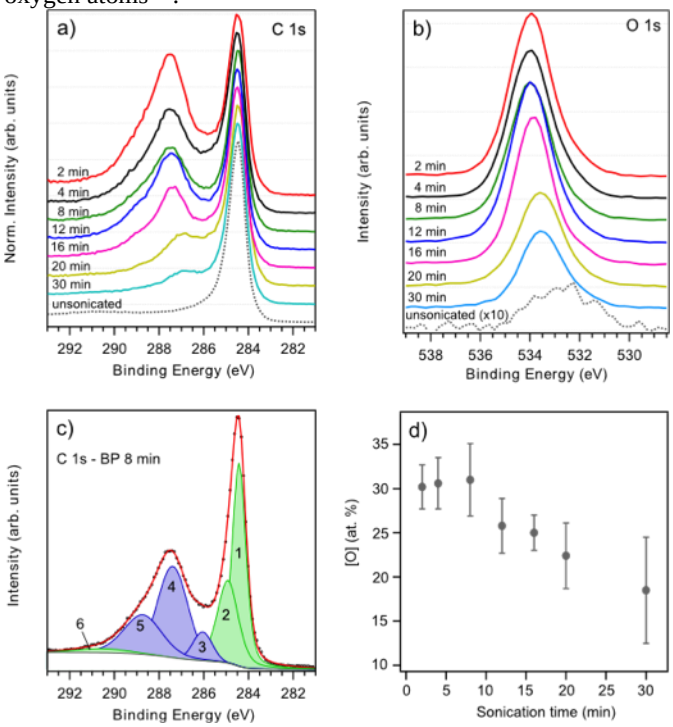

Figure 7. Typical XPS survey spectra recorded on unsonicated VGCNFs (black line) and Buckypapers (BP) produced from dispersions prepared using 2 min and 30 min of sonication (red and blue line, respectively).

To reproduce the C1s peak recorded after 8 min of sonication (Figure 7c), 6 components were used. Only three components (1, 2 and 6, Figure 7c) are required for fitting the spectrum of pristine (unsonicated) VGCNF: in addition to the asymmetric sp^2 peak at 284.4 eV, two Gaussian functions were used to reproduce the other features observed in the pristine spectrum. One Gaussian at 285.0 eV is associated with photoelectrons emitted from carbon atoms at sp^3 bonds in amorphous carbon. During VGCNF synthesis, competing pathways can lead to amorphous carbon formation rather than to crystalline graphitic nanofibres (as discussed in electron microscopy section, see also Figure 1b-c). The other Gaussian, centred at 290.6 eV, corresponds to the π-plasmon excitations. The three other Gaussian components (3 to 5, Figure 7c) are related to oxygen containing functional groups present in gellan gum, and centered at 286.1 eV (hydroxilic), 287.2 eV (carbonylic) and 288.6 eV (carboxylic). It is clear from Figure 7a that the broad structure at 288 eV decreases with increasing sonication. In addition, the O1s peak (previously observed for modified gellan gum[67]) is also decreasing with increasing sonication time (Figure 7b). In other words, the amount of oxygen containing groups is decreasing near the surface of the VGCNFs as shown in Figure 7d. The relative amount of oxygen in the unsonicated sample was evaluated to be 2%.

XPS is predominantly a surface technique (about 8 nm depth of analysis). Combined with the diameter of the VGCNF this would suggest that XPS can only provide data about the surface of the VGCNF and not the interior. Hence, it is suggested that the observed decrease in the O1s spectra (Figure 7b) and the oxygen containing groups in the C1s spectra (Figure 7d) can be explained by the reduction of gellan gum on, or near the surface of VGCNF due to filling of the VGCNF with gellan gum. Electron microscopy results (Figure 1) appear to be in support of this suggestion, with the fibres becoming filled to a larger extent with increasing sonication time.

Conclusions

Incorporation of tubular carbon nanostructures into materials to form hybrid materials is an attractive area of chemical materials research. Tailoring the properties using sonication of functionalised materials is potentially very exciting as this allows for both physical and/or chemical changes.

The effect of sonolysis on vapour grown carbon nanofibers in gellan gum composite materials has been investigated. Finding the minimum time for sonication is a typical first step when producing dispersions containing carbon nanostructures, however rarely is the effect of sonolysis on the properties of the constituents and the resulting materials studied in detail.

It was found that the average length of the VGCNFs was halved with just 30 minutes of low energy sonication. Electron microscopy analysis revealed that the VGCNFs were opened, shortened and filled. Spectroscopy analysis revealed that sonication treatment resulted in modification of the VGCNFs.

Our investigations revealed that the electrical characteristics reduced (from 35 ± 2 S/cm to 25 ± 2 S/cm) due to sonication-induced reduction in length of the carbon nanofibers. In contrast, it is likely that the reduction in mechanical characteristics is mostly due to the effect of sonolysis on polymer chain length.

This paper demonstrates that despite the sonication-induced opening, filling and modification of carbon nanofibers composite materials that are mechanical robust and electrically conducting can be easily prepared by limiting the amount of horn sonolysis (to just 4 min).

Methods for the filling of carbon nanotubes are well established, there has been limited research regarding the filling of carbon nanofibers[62,68]. One of the remaining challenges is to prepare filled tubular carbon nanostructures with properties suitable for selective drug delivery (e.g. nanosized needles) and for autonomic healing of polymeric materials (e.g. load-bearing biomedical materials). It is suggested that filled VGCNFs offer great opportunities for addressing these challenges.

Acknowledgements

This project was supported by the University of Wollongong (UOW), Australian Research Council (ARC) Centre of Excellence for Electromaterials Science, ARC Future Fellowship program, and the Belgian Fund for Scientific Research (FRS-FNRS) under FRFC contract “Chemographene” (convention N°2.4577.11). Carla Bittencourt and Marc in het Panhuis acknowledge support from the European Union COST action MP0901 “NanoTP” and Australia Academy of Science. Ross Clark (CP Kelco) and Patricia Hayes (UOW) are thanked

for the provision of gellan gum and assistance with Raman measurements. The authors acknowledge the use of facilities within the UOW Electron Microscopy Centre and the Materials Node of the Australia National Fabrication Facility.

Notes and references

1. Soft Materials Group, School of Chemistry, University of Wollongong, Wollongong, NSW 2522, Australia
2. Chimie des Interactions Plasma Surface, CIRMAP, University of Mons, Place du Parc 20, 7000 Mons, Belgium
3. Electron Microscope Centre, AIIM Facility, University of Wollongong, Wollongong, NSW 2522, Australia
4. Intelligent Polymer Research Institute, ARC Centre of Excellence for Electromaterials Science, AIIM Facility, University of Wollongong, Wollongong, NSW 2522, Australia.

* Corresponding author. E-mail address: panhuis@uow.edu.au (M. in het Panhuis)

References

1. C.-H. Kiang, J.-S. Choi, T. T. Tran, and A. D. Bacher, *J. Phys. Chem. B*, 1999, **103**, 7449–7451.
2. D. Ugarte, T. Stöckli, J. M. Bonard, A. Châtelain, and W. A. de Heer, *Appl. Phys. A Mater. Sci. Process.*, 1998, **67**, 101–105.
3. P. M. Ajayan and S. Iijima, *Nature*, 1993, **361**, 333–334.
4. Y. Chen, D. T. Shaw, X. D. Bai, E. G. Wang, C. Lund, W. M. Lu, and D. D. L. Chung, *Appl. Phys. Lett.*, 2001, **78**, 2128–2130.
5. G. Che, B. B. Lakshmi, C. R. Martin, and E. R. Fisher, *Langmuir*, 1999, **15**, 750–758.
6. X. Pan and X. Bao, *Chem. Commun.*, 2008, 6271–6281.
7. A. Leonhardt, S. Hampel, C. Müller, I. Mönch, R. Koseva, M. Ritschel, D. Elefant, K. Biedermann, and B. Büchner, *Chem. Vap. Depos.*, 2006, **12**, 380–387.
8. G. Korneva, H. Ye, Y. Gogotsi, D. Halverson, G. Friedman, J.-C. Bradley, and K. G. Kornev, *Nano Lett.*, 2005, **5**, 879–884.
9. M. Majumder, N. Chopra, and B. J. Hinds, *J. Am. Chem. Soc.*, 2005, **127**, 9062–9070.
10. S. A. Miller and C. R. Martin, *J. Am. Chem. Soc.*, 2004, **126**, 6226–7.
11. D. Du, M. Wang, Y. Qin, and Y. Lin, *J. Mater. Chem.*, 2010, **10**, 1532–1537.
12. M. Whitby and N. Quirke, *Nat. Nanotechnol.*, 2007, **2**, 87–94.
13. B. M. Kim, S. Qian, and H. H. Bau, *Nano Lett.*, 2005, **5**, 873–878.
14. X. P. Gao, Y. Zhang, X. Chen, G. L. Pan, J. Yang, F. Wu, H. T. Yuan, and D. Y. Song, *Carbon*, 2004, **42**, 47–52.
15. W. Hu, D. Gong, Z. Chen, L. Yuan, K. Saito, C. A. Grimes, and P. Kichambare, *Appl. Phys. Lett.*, 2001, **79**, 3083–3085.
16. J. Sloan, J. Hammer, M. Zwiefka-Sibley, and M. L. H. Green, *Chem. Commun.*, 1998, 347–348.
17. S. C. Tsang, P. J. F. Harris, and M. L. H. Green, *Nature*, 1994, **372**, 159–162.
18. P. M. Ajayan, T. W. Ebbesen, and T. Ichihashi, *Nature*, 1993, **362**, 522–525.
19. O. Byl, P. Kondratyuk, S. T. Forth, S. a FitzGerald, L. Chen, J. K. Johnson, and J. T. Yates, *J. Am. Chem. Soc.*, 2003, **125**, 5889–96.
20. B. C. Satishkumar, A. Govindaraj, J. Mofokeng, G. N. Subbanna, and C. N. R. Rao, *J. Phys. B At. Mol. Opt. Phys.*, 1996, **29**, 4925–4934.
21. G. Tang, D. Chang, D. Wang, J. He, W. Mi, J. Zhang, and W. Wang, *Polym. Plast. Technol. Eng.*, 2012, **51**, 377–380.
22. J. E. Puskas, E. A. Foreman-Orlowski, G. T. Lim, S. E. Porosky, M. M. Evancho-Chapman, S. P. Schmidt, M. El Fray, M. Piątek, P. Prowans, and K. Lovejoy, *Biomaterials*, 2010, **31**, 2477–2488.
23. X. Chen, S. Wei, A. Yadav, R. Patil, J. Zhu, R. Ximenes, L. Sun, and Z. Guo, *Macromol. Mater. Eng.*, 2011, **296**, 434–443.
24. Y. Yang, M. C. Gupta, K. L. Dudley, and R. W. Lawrence, *Nanotechnology*, 2004, **15**, 1545–1548.
25. L. Vaisman, H. D. Wagner, and G. Marom, *Adv. Colloid Interface Sci.*, 2006, **128-130**, 37–46.
26. J. Xu, S. Chatterjee, K. W. Koelling, Y. Wang, and S. E. Bechtel, *Rheol. Acta*, 2005, **44**, 537–562.
27. F. Hennrich, R. Krupke, K. Arnold, J. A. Rojas Stütz, S. Lebedkin, T. Koch, T. Schimmel, M. M. Kappes, and J. A. R. Stu, *J. Phys. Chem. B*, 2007, **111**, 1932–1937.
28. S. Kumar, B. Lively, L. L. Sun, B. Li, and W. H. Zhong, *Carbon*, 2010, **48**, 3846–3857.
29. Q. Cheng, S. Debnath, E. Gregan, and H. J. Byrne, *J. Phys. Chem. C*, 2010, **114**, 8821–8827.
30. K. L. Lu, R. M. Lago, Y. K. Chen, M. L. H. Green, P. J. F. Harris, and S. C. Tsang, *Carbon*, 1996, **34**, 814–816.
31. E. S. K. Tang, M. Huang, and L. Y. Lim, *Int. J. Pharm.*, 2003, **265**, 103–114.
32. P. He, Y. Gao, J. Lian, L. Wang, D. Qian, J. Zhao, W. Wang, M. J. Schulz, X. P. Zhou, and D. Shi, *Compos. Part A Appl. Sci. Manuf.*, 2006, **37**, 1270–1275.
33. P. Vichchulada, M. A. Cauble, E. A. Abdi, E. I. Obi, Q. Zhang, and M. D. Lay, *J. Phys. Chem. C*, 2010, **114**, 12490–12495.
34. G. J. Price, *Ultrason. Sonochem.*, 1996, **3**, S229–S238.
35. D. Hecht, L. Hu, and G. Grüner, *Appl. Phys. Lett.*, 2006, **89**, 133112.
36. S. Koda, K. Taguchi, and K. Futamura, *Ultrason. Sonochem.*, 2011, **18**, 276–281.
37. J. P. Lorimer, T. J. Mason, T. C. Cuthbert, and E. A. Brookfield, *Ultrason. Sonochem.*, 1995, **2**, S55–S57.
38. G. J. Price and P. F. Smith, *Polymer*, 1993, **34**, 4111–4117.
39. M. L. Tsaih and R. H. Chen, *J. Appl. Polym. Sci.*, 2003, **90**, 3526–3531.
40. A. J. Granero, J. M. Razal, G. G. Wallace, and M. in het Panhuis, *Adv. Funct. Mater.*, 2008, **18**, 3759–3764.
41. A. Aldalbahi and M. in het Panhuis, *Carbon*, 2012, **50**, 1197–1208.
42. E. R. Morris, K. Nishinari, and M. Rinaudo, *Food Hydrocoll.*, 2012, **28**, 373–411.
43. I. B. Bajaj, S. A. Survase, P. S. Saudagar, and R. S. Singhal, *Food Technol. Biotechnol.*, 2007, **45**, 341–354.
44. L. Lu and W. Chen, *ACS Nano*, 2010, **4**, 1042–8.
45. C. J. Ferris and M. in het Panhuis, *Soft Matter*, 2009, **5**, 1466–1473.
46. H. Warren, R. D. Gately, P. O'Brien, R. Gorkin, and M. in het Panhuis, *J. Polym. Sci. Part B: Polym. Phys.*, 2014, **52**, 864-871.
47. J. P. Ferrance, *Electroanalysis*, 2011, **23**, 2906 – 2914.
48. T. V Hughes and C. R. Chambers, 1889, Manufacture of Carbon Filaments, U.S. Patent 405,480.
49. L. V Radushkevich and V. M. Lukyanovich, *Zurn. Fis. Chim.*, 1952, **26**, 88–95.
50. M. Endo, Y. Kim, T. Hayashi, K. Nishimura, T. Matusita, K. Miyashita, and M. Dresselhaus, *Carbon*, 2001, **39**, 1287–1297.

51. T. Uchida, D. P. Anderson, M. L. Minus, and S. Kumar, *J. Mater. Sci.*, 2006, **41**, 5851–5856.
52. M. Endo, Y. A. Kim, T. Hayashi, Y. Fukai, K. Oshida, M. Terrones, T. Yanagisawa, S. Higaki, and M. S. Dresselhaus, *Appl. Phys. Lett.*, 2002, **80**, 1267–1269.
53. J. Y. Howe, G. G. Tibbetts, C. Kwag, and M. L. Lake, *J. Mater. Res.*, 2006, **21**, 2646–2652.
54. J. Ding, Y. Zhu, and Y. Fu, *Polym. Compos.*, 2014, **35**, 412–417.
55. M. D. Sanchez-Garcia, J. M. Lagaron, and S. V Hoa, *Compos. Sci. Technol.*, 2010, **70**, 1095–1105.
56. M. Hosur, R. Barua, S. Zainuddin, S. Jeelani, A. Kumar, J. Trovillion, and Y. Pereza, *Matéria (Rio Janeiro)*, 2010, **15**, 247–253.
57. P. Cardoso, J. Silva, A. J. Paleo, F. W. J. van Hattum, R. Simoes, and S. Lanceros-Méndez, *Phys. Status Solidi*, 2010, **207**, 407–410.
58. M. Chipara, R. A. Vaia, and A. Nasar, *Vacuum*, 2014, **107**, 254-258.
59. A. Khattab, C. Liu, W. Chirdon, and C. Hebert, *J. Thermoplast. Compos. Mater.*, 2012, **26**, 954–967.
60. H. D. Deshpande, D. R. Dean, V. Thomas, W. C. Clem, M. V Jose, E. Nyairo, and M. Mishra, *Curr. Nanosci.*, 2012, **8**, 753–761.
61. J.-M. Thomassin, C. Jérôme, T. Pardoen, C. Bailly, I. Huynen, and C. Detrembleur, *Mater. Sci. Eng. R*, 2013, **74**, 211–232.
62. M. Monthioux, *Carbon*, 2002, **40**, 1809–1823.
63. F. Tuinstra and J. L. Koenig, *J. Compos. Mater.*, 1970, **4**, 492–499.
64. A. Sesis, M. Hodnett, G. Memoli, A.J. Wain, I. Jurewicz, A.B. Dalton, J.D. Carey and G. Hinds, *J. Phys. Chem. B*, 2013, **117**, 15141-15150.
65. S. Hufner, *Photoelectron spectroscopy: Principles and applications*, Springer-Verlag, New York, 3rd edn., 2003.
66. T. Ohno, T. Tsubota, M. Toyofuku, and R. Inaba, *Catal. Letters*, 2004, **98**, 255–258.
67. D.F. Coutinho, S. Sant, M. Shakiba, B. Wang, M.E. Gomes, N.M. Reves, R.L. Reis, and A. Khademhosseini, *J. Mater. Chem.*, 2012, **22**, 17262-17271.
68. R.D. Gately and M. in het Panhuis, Beilstein J. Nanotechnol., 2015, "Filling of carbon nanotubes and nanofibers", in press.